Contents lists available at ScienceDirect

International Journal of Applied Earth Observations and Geoinformation

The first fine-resolution mapping of contour-levee irrigation using deep Bi-Stream convolutional neural networks

Lu Liang [a,*,1], Abolfazl Meyarian [b,1], Xiaohui Yuan [b,*], Benjamin R.K. Runkle [c], George Mihaila [b], Yuchu Qin [d], Jacob Daniels [e], Michele L. Reba [f], James R. Rigby [g]

[a] Department of Geography and the Environment, University of North Texas, Denton, TX 76203, USA
[b] Department of Computer Science and Engineering, University of North Texas, Denton, TX 76203, USA
[c] Department of Biological and Agricultural Engineering, University of Arkansas, Fayetteville, AR 72701, USA
[d] State Key Laboratory of Remote Sensing Science, Aerospace Information Research Institute, CAS, Beijing 100101, China
[e] Department of Electrical Engineering, University of North Texas, Denton, TX 76203, USA
[f] Delta Water Management Research Unit, USDA-Agricultural Research Service, Jonesboro, AR 72401, USA
[g] USDA-ARS National Sedimentation Laboratory, Oxford, MS 38655, USA

ARTICLE INFO

ABSTRACT

Agricultural irrigation accounts for nearly 70% of global freshwater withdrawal. Among irrigation practices, contour-levee cascade irrigation is of particular interest as it is water-intensive and widely used in many rice production regions. Despite its significant environmental implications, no study has quantified the distribution of contour-levee irrigation. One major challenge of remote sensing-based contour-levee field detection is how to accurately identify the thin and curved levee lines whose appearance varies dramatically in different fields. This paper presents a new deep network-based method that jointly optimizes semantically meaningful features to quantify the contour-levee fields. This new method uses a bi-stream encoder-decoder architecture to capture spectral information and gradient features. To maintain image gradient sharpness, a skip connection approach is employed to facilitate gradient propagation across long-range connections. Moreover, the new method uses deep supervision to generate more informative features from the earlier hidden layers and superpixel segmentation to reduce classification noise as a post-processing step. By testing against 41 images across 10 Arkansas counties, the average accuracy was 86.23% and the method achieved 15%-17% improvement over benchmark methods. The results show that IrrNet-Bi-Seg maintains good transferability and is thus promising for larger-scale applications.

1. Introduction

Irrigated agriculture represents 20% of cultivated land and accounts for 40% of global crop production (UNESCO, 2014) and nearly 70% of freshwater withdrawals globally (Molden et al., 2007). Effective water resources management requires accurate quantification of irrigation water usage and efficiency, which are synergistically related to the irrigation method and land form (Hsiao et al., 2007). A natural focus for advancing this goal is a spatially explicit accounting of fields using the contour-levee irrigation strategy—the most water-intensive yet widely used method by some major crops, such as rice and soybean (Massey et al., 2017). In contour-levee fields, water flows by gravity from upper to lower fields, and levees are used to maintain inundation to control weed growth. Thus, an excessive amount of water is drained off by gravity and wasted (Massey et al., 2018; Vories et al., 2005). The irrigation application rate for contour-levee fields is 8%-14% or 46–57% higher than some newer flooding methods, such as straight levee or zero grade, respectively (Henry et al., 2016; Massey et al., 2017; Reba and Massey, 2020). Knowing the distribution of contour-levee fields is a fundamental step to assess their impact on the regional hydrological cycle and is critically important to provide stakeholders information to understand and manage water resources and other sustainability metrics (Moreno-García et al., 2021).

Historically, irrigated land area is reported through the Irrigation

---

* Corresponding authors.
  E-mail address: lu.liang@unt.edu (L. Liang).
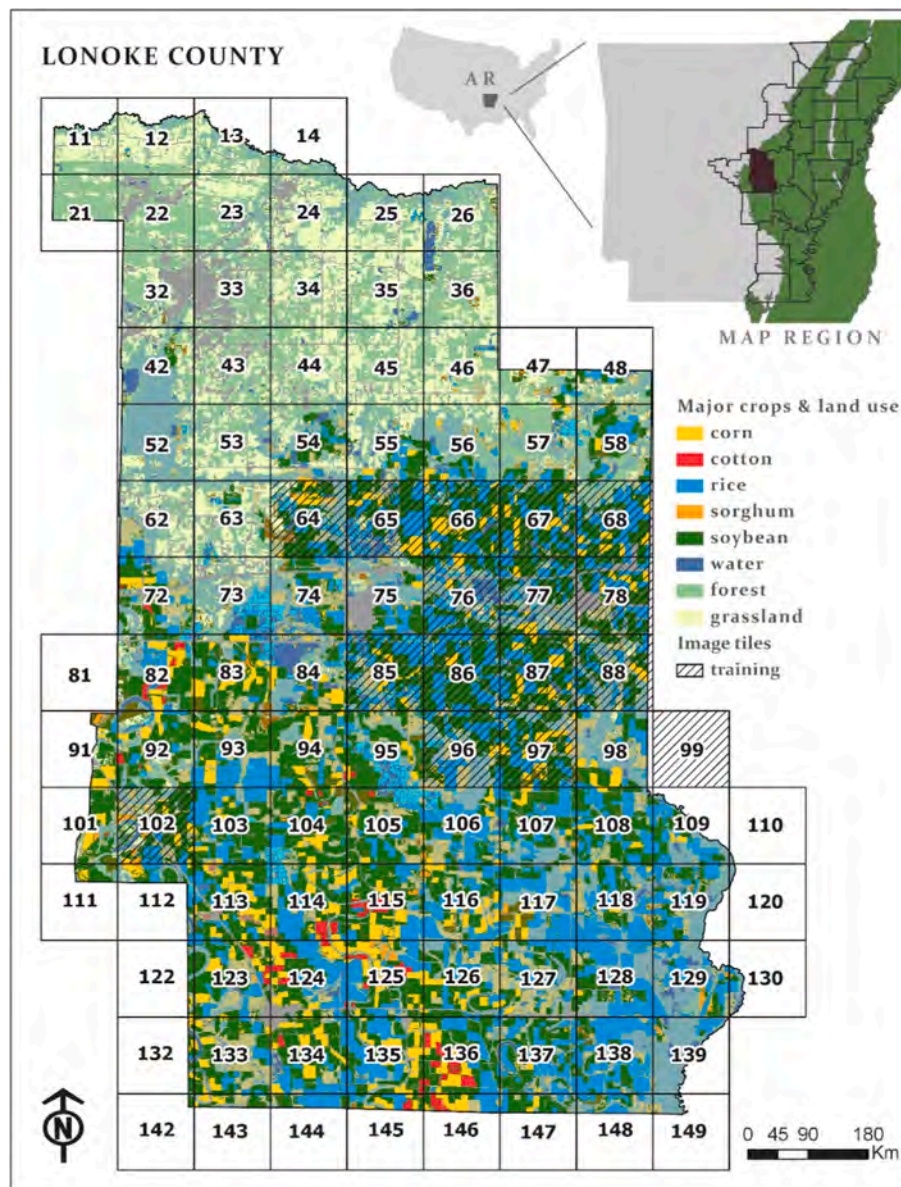[1] The authors contributed equally.

Fig. 1. The Lonoke County, Arkansas, and the 27 Arkansas counties covering the Mississippi Alluvial Plain region. Lonoke County was seamlessly cropped into numbered image tiles and overlain on the 2015 Cropland Data Layer. Edge tiles with no valid pixel values are not mapped.

and Water Management Survey, but this tabular data is less informative about its spatial distribution. Remote sensing technique can demarcate the extent of irrigated lands at various scales (Ketchum et al., 2020; Pervez and Brown, 2010; Thenkabail et al., 2009; Xie et al., 2021), but methods to classify irrigation types are underdeveloped due to the complex visual characteristics of different geometry, photometry, and texture in various irrigation types. The center pivot is widely mapped because its simple and distinct large circular shape is easily captured by satellite or aerial images (Rundquist et al., 1989; Yan and Roy, 2014). Despite the significant ecological and environmental implications of contour-levee irrigation, its spatial distribution is rarely known. The major challenges are that different contour-levee fields pose distinct image color and texture, and the levee appearance (e.g., spacing between levees and levee width) varies dramatically in different fields. Traditional pixel-based methods thus have difficulty incorporating textural features (e.g., contour-levee) in making predictions (Jawak et al., 2015). Object-based image analysis is also not viable as field contours are diverse in shape and would require repeated tests and trials in parameter optimization (Yang et al., 2019a,b).

The integration of deep learning (DL) and very-high-resolution images have emerged as a promising solution considering their combined ability to optimize semantically meaningful feature extraction and classification (Mi and Chen, 2020). Here, we present a novel DL approach named IrrNet-Bi-Seg for the automatic detection of contour-levee agricultural fields with the following highlights. First, it used pre-trained model to reduce the effort of developing a large training dataset for classification on new images. Second, its bi-stream network architecture fused both spectral and textural information. Third, skip connection and deep supervision are incorporated in the deep multilayer network to address the gradient vanishing challenge. Fourth, image segmentation was used in the post-processing to suppress classification noise. Using this approach, we provide a comprehensive assessment of the distribution of contour-levee irrigation for the state of Arkansas, which also tests whether a generalized DL model developed and calibrated at a local scale is suitable for application at a larger scale or in a different region. This first study of its kind is of great importance to evaluating the environmental, ecological, and societal impacts of this prevalent irrigation system type, and to providing stakeholders and
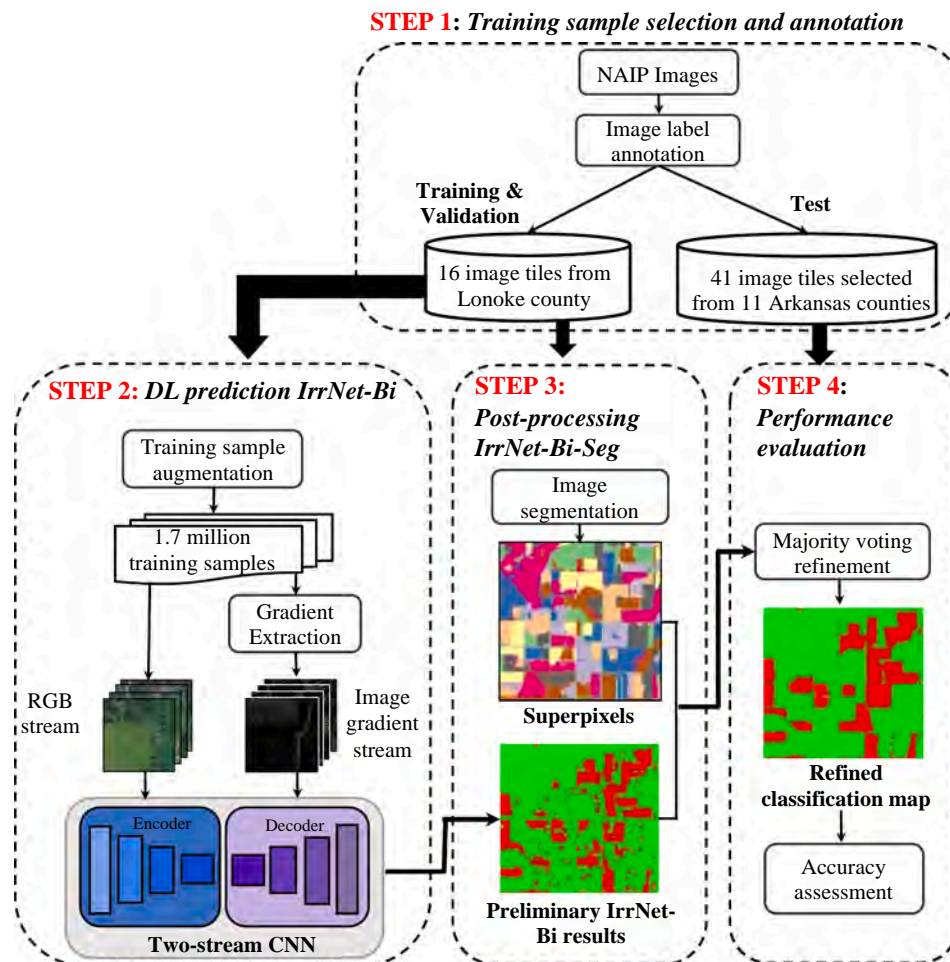
2

STEP 1: *Training sample selection and annotation*

Fig. 2. Proposed deep learning and image segmentation fused system detection workflow (IrrNet-Bi-Seg).

managers information to better understand and manage water resources.

2. Study area and data

2.1. Study area

Our study area is the Mississippi Alluvial Plain (MAP) region of Arkansas (Fig. 1). This highly productive agricultural region encompasses nearly 14 million acres of cropland across 27 counties (Fig. 1, "USDA/NASS 2020 State Agriculture Overview for Arkansas," 2020). In particular, Arkansas is the top US rice producer and approximately half of its total rice acres use contour-levee irrigation (Wilson and Branson, 2004). The dry season coincides with the rice-growing season, which usually starts from late March to mid-May and lasts till mid-August to mid-October (Liang et al., 2019). As a result, irrigation has surged in demand. Between 1992 and 1997, the irrigated area increased by 438,553 ha (Reba and Massey, 2020). Given the projected changes in drought frequency and crop water needs (Yang et al., 2019a,b) and large uncertainty in the distribution and timing of water availability (Gosling and Arnell, 2016), irrigation water use will increasingly compete with natural ecosystem and municipal water needs in this region.

2.2. High-resolution aerial NAIP imagery

A typical field usually only has 3 to 10% of the land in levees that are 28 to 33 cm wide (California Rice Production Workshop, 2018). Due to their thin serpentine nature, levee features can barely be visualized on medium or coarse-resolution satellite images (Figure S1). We used the United States Department of Agriculture (USDA) National Agriculture Imagery Program (NAIP) aerial imagery acquired during the agricultural growing season of 2015 at a 1 m resoluiton to discern field-level details (free access at https://datagateway.nrcs.usda.gov/). Because no significant increase in accuracy was found when DL algorithms trained on multispectral images were applied over their natural-color counterpart (Salamati et al., 2012), we used the three natural color bands (Red, Green, and Blue) to reduce data volume and increase transferability to other data sources.. We cropped the image covering Lonoke into 149 tiles at the dimension of 5000 × 5000 pixels leading to each image capturing 25 km^2 (Fig. 1). For the entire MAP region, there are 4,229 image tiles.

3. Proposed method

3.1. Training sample selection, label annotation, and augmentation

We used manual annotation to build a training database of irrigation practice types following previous protocols (Liang et al., 2016). Because contour-levee irrigation is strongly associated with rice and soybean cultivation, we selected 16 representative tiles from Lonoke County (Fig. 1)—the largest rice production county in Arkansas and 99% of its irrigated croplands use surface flooding irrigation (Dieter et al., 2018). For test samples, we picked 41 tiles from 11 counties in Arkansas's MAP region for an independent assessment (Fig. 2, Step 1).

To boost annotation efficiency, we used a web-based image annotation tool Label4RS based upon an open-source program Label Studio
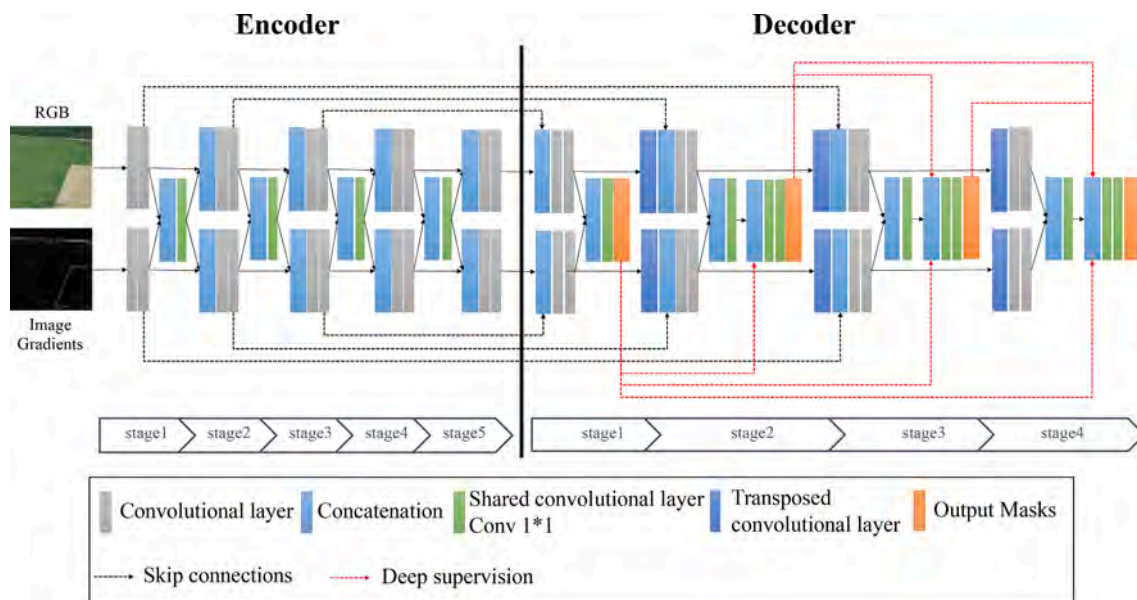
Fig. 3. The bi-stream convolutional neural network architecture of IrrNet-Bi.

(Tkachenko et al., 2020) (Supplementary File 1). Contour-levee fields display curved lines with irregular intervals that seem to resemble a topographical pattern (Figure S1). All other irrigation systems (e.g., straight-levee, center-pivot, and zero-grade), non-irrigated and non-agricultural lands are considered as background. The annotation started with boundary delineation of contour-levees fields by wall to wall examination. Fields that were difficult to classify were revisited by a second analyst. Three rounds of annotation and quality control were conducted independently. The agreement between different annotations was measured by the Cohen Kappa score (Cohen, 1960). The average Cohen Kappa score across all annotated images is 0.84, which indicates high annotation reliability (Artstein and Poesio, 2008).

The labeling process identified 23.75% of the total pixels as contour-levee fields and the rest (76.25%) as background. Because the class distribution's skew could induce a class-imbalance problem, we rotated the original image tiles every 5 degrees from 0 to 180 degrees to generate additional images with different views. Sub-sample images at 300 × 300 size were then extracted using a sliding window strategy. The window was convolved over the images with a stride of 40 pixels and the region encompassed by the window was selected. We generated more than 1.7 million samples out of the 16 image tiles and we took an equal number of samples from each class to balance the data distribution. A total of 200,000 were randomly selected to train the model.

3.2. Two-stream convolutional neural network IrrNet-Bi

3.2.1. Bi-stream encoder-decoder convolutional network IrrNet-Bi

To overcome the challenge in field levee recognition caused by variation of image color and texture from irrigation scheduling, crop type, and varied levee appearance, a bi-stream CNN IrrNet-Bi that processes RGB images and image gradients is implemented (Fig. 2 Step 2; Fig. 3). The RGB stream takes the color image as the input, whereas the other stream uses image gradients from the intensity (Meyarian et al., 2021). Both streams have encoder and decoder layers, and shared convolution layers are used to share feature maps. In the encoder network, the RGB and image gradient data are first processed through two convolutional layers, the results of which are concatenated and passed to the next layer, allowing feature incorporation from each stream and reducing the feature map's dimensionality. The outcomes of this convolution layer feed to the next units of both streams.

Supplementary File 2 gives two examples to demonstrate how bi-stream data fusion benefits the process.

Gradient vanishing, where a deep multilayer network fails to propagate useful updates to the layers near the input of the network, is a common challenge in DL (Ronneberger et al., 2015). We employed skip connections to facilitate gradient propagation across deep layers by passing the outputs from three levels of the encoder to the decoder (Fig. 3). The combined usage of low-level features from the encoder and high-level features of the decoder allows the integration of both detailed and abstract features, leading to more accurate predictions (Huang et al., 2018; Ronneberger et al., 2015).

Another key improvement in IrrNet-Bi is deep supervision, which provides an integrated loss function as a means to directly supervise the earlier hidden layers, rather than only the output layers (Xie and Tu, 2015). This step forces the decoder to generate more informative features in a way that the final output mask balances information from earlier and later input layers. At each of the four prediction stages in the decoder, the feature maps generated by both streams are concatenated and then processed by the next convolutional layer (Fig. 3). Due to the size variance of the first three predicted masks, a bilinear upsampling is used to match the mask size with the size of the annotated image. Finally, the predicted masks are compared against the annotated image to calculate the overall loss.

3.2.2. Loss function

The loss function C is a weighted summation of the individual loss at all stages, comparing the generated prediction with the annotated masks (Eq.1):

$$C = \sum_{i=1}^{4} \lambda_i \times \Gamma(G, M_i) + L_r \tag{1}$$

where G is the annotated mask for a given image; M_i is the output at the ith stage of the decoder; λ_i is the weight associated with the output for each level of prediction in the decoder; $\Gamma(\bullet)$ is a Softmax cross-entropy function for binary classification (Eq.2):

$$\Gamma(G, M_i) = \frac{1}{N} \sum_{x,y} - (G(x, y) \times \log(M_i(x, y)) + (1 - G(x, y)) \times \log(1$$
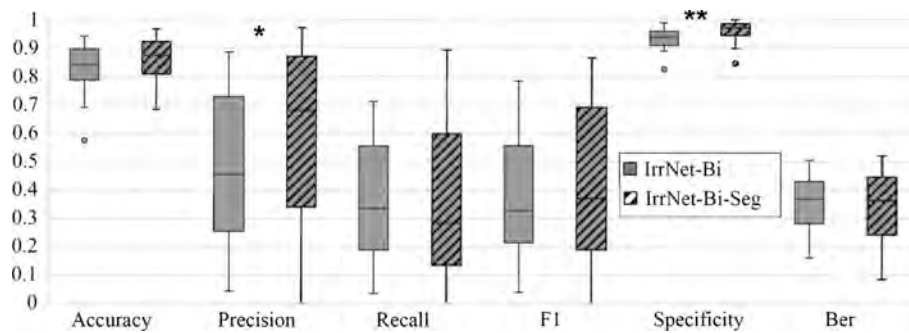$$- M_i(x, y))) \tag{2}$$

Fig. 4. Boxplots displaying the accuracy assessment reported by IrrNet-Bi and IrrNet-Bi-Seg using 41 independent test samples. The bottom and top of the box are the first and third quantiles, and the band inside the box is the median. Asterisks on top of the accuracy group indicate that the difference between the means of IrrNet-Bi and IrrNet-Bi-Seg accuracy values is statistically significant.*: p-value < 0.05; **: p-value < 0.01;.

where N is the total number of pixels; $G(x, y)$ is the annotated label at (x, y) pixel, i.e., one for contour-levee fields and zero for background; $M_i(x, y)$ are the predicted probability of contour-levee for the pixel at (x, y). The weight λ_i is decided empirically. To regularize the network parameters, L2-norm is used:

$$L_r = \lambda_R \times \sum_{i=1}^{N} w_i^2$$

where λ_R is the regularization coefficient, empirically set to 10^{-5} here, that controls the amount of contribution of the L2-norm; w_i is the weight parameters. The weights of the network are initialized randomly.

3.3. Superpixel-enhanced post-processing

Given the detailed spatial information contained in the NAIP imagery that can cause large variation of spatial structures, a post-processing superpixel segmentation step is introduced to reduce classification noise and to sharpen field boundaries (Fig. 2 Step 3). We tested four mainstream image segmentation techniques, separately: simple linear iterative clustering (Achanta et al., 2010), quick shift (Vedaldi and Soatto, 2008), Felzenswalb and Huttenlocher (Felzenszwalb and Huttenlocher, 2004), and compact watershed (Neubert and Protzel, 2014). We downsized the original 5000 × 5000 resolution to 100 × 100, 200 × 200, 300 × 300, 400 × 400, and 500 × 500 using bilinear interpolation to suppress fine details. Note that the downsized images are only used for image segmentation and not for the IrrNet-Bi model. We used the shape elongation term E(S) to remove superpixels with elongated shapes to avoid false-positive predictions (Stojmenović and Žunić, 2008). The detailed process is provided in Supplementary File 3. For each superpixel, a majority voting evaluation is performed among the pixel-wise DL predictions to generate the final classification IrrNet-Bi-Seg.

3.4. Performance evaluation

We evaluated model performance in four ways (Fig. 2 Step 4). We first used ten-fold validation to estimate the skill of a new model on unseen data using the 16 training tiles. Then, we used the 41 independent test image samples to provide an unbiased estimate of the final tuned model. A set of pixel-level accuracy metrics were used, including *Accuracy, Precision, Recall, F₁, Specificity*, and *Balanced Error Rate (BER)*, as described in the Supplementary File 4. Moreover, we evaluated the network without the inclusion of image gradient stream—leaving only the RGB stream as the input feature (named as IrrNet-RGB-Seg model). Finally, we adopt two benchmark methods including Random Forest (RF) and FCN-ATR-SKIP for comparison. RF (Breiman, 2001) is often established as a baseline model in land cover mapping (e.g., Liang et al., 2016). FCN-ATR-SKIP is a fully convolutional network that is made of atrous convolutional layers and exploits contextual information (Mboga et al., 2020), which has proven robustness to poor radiometric quality

Table 1

Performance comparison of random forest, FCN-ATR-SKIP, and IrrNet-Bi-Seg based on the 16-fold validation and accuracy assessment using 41 independent test samples. The average values of each metric alongside the standard deviation were reported.

Model	Accuracy	BER	Precision	Recall	F1	Specificity
16-fold validation						
IrrNet-Bi-Seg	0.90 ± 0.07	0.17 ± 0.09	0.80 ± 0.11	0.73 ± 0.18	0.75 ± 0.15	0.94 ± 0.05
Independent test						
Random Forest	0.76 ± 0.07	0.44 ± 0.09	0.21 ± 0.18	0.29 ± 0.23	0.21 ± 0.16	0.82 ± 0.08
FCN-ATR-SKIP	0.81 ± 0.09	0.44 ± 0.09	0.25 ± 0.02	0.25 ± 0.21	0.21 ± 0.17	0.88 ± 0.09
IrrNet-RGB-Seg	0.81 ± 0.09	0.39 ± 0.11	0.40 ± 0.28	0.29 ± 0.22	0.29 ± 0.22	0.92 ± 0.05
IrrNet-Bi	0.83 ± 0.08	0.35 ± 0.10	0.49 ± 0.26	0.36 ± 0.20	0.39 ± 0.20	0.93 ± 0.04
IrrNet-Bi-Seg	0.86 ± 0.08	0.34 ± 0.13	0.61 ± 0.29	0.37 ± 0.27	0.41 ± 0.28	0.96 ± 0.04

and could be suitable for the NAIP images that lack atmospheric and radiometric corrections. We trained and tested both RF and FCN-ATR-SKIP models in the same way as IrrNet-Bi-Seg model.

4. Results

4.1. Evaluation of image segmentation performance

After performing a visual comparison of the image segmentation results generated by four different methods on a series of downscaled images, the Felzenswalb and Huttenlocher algorithm achieved the best results on the downscaled 12.5 m resolution image (Supplementary File 3). By testing on 41 independent test tiles, the slightly increased *Accuracy* from 0.83 to 0.86 indicated overall improvement of IrrNet-Bi-Seg over IrrNet-Bi, though the difference is not significant using a paired *t*-test at the significance level of 0.05 (Fig. 4). *Precision*, which quantifies how well the contour-levee fields have been classified, has significant improvement from an average of 0.49 to 0.61. The other metrics, other than *Specificity*, do not show significant differences in the values. However, these results should not imply that the superpixel processing does not affect the mapping results, which are discussed in the next section. The non-significant changes in metric values could derive from their calculation on a pixel basis. While superpixels can remove some
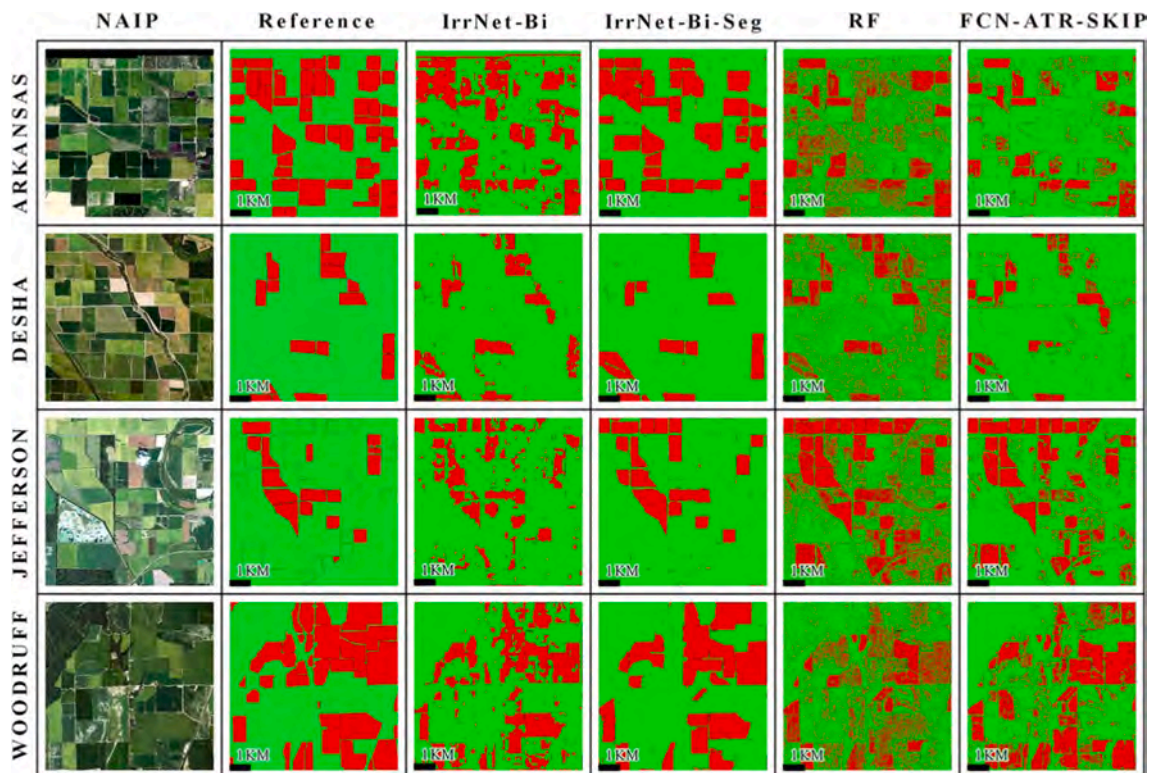
Fig. 5. Comparison of contour-levee field predictions generated from IrrNet-Bi, IrrNet-Bi-Seg, and the two benchmark methods RF and FCN-ATR-SKIP. NAIP column displays the 5000 × 5000 NAIP images at which those models are tested. The reference column represents all the annotated labels. All red pixels indicate the contour-levee fields and green pixels are backgrounds. (For interpretation of the references to color in this figure legend, the reader is referred to the web version of this article.)

falsely classified pixels if most of their pixels were correctly classified, errorous superpixels can add false positive pixels. Overall, the number of corrected pixels slightly surpasses the number of miscorrected pixels, as evidenced by the marginally increased accuracy values.

4.2. Performance evaluation and benchmark comparison

The 16-fold cross-validation reported the mean *accuracy* of 0.90, mean BER at 0.17, and *F1* score of 0.75 (Table 1). The relatively high accuracy and low error imply that IrrNet-Bi-Seg can generally perform well when used to make predictions on data not used during the training phase, which was further confirmed by the independent accuracy assessment. Image gradient stream benefited the model, as evidenced by the increased values of all five accuracy metrics and decreased BER from IrrNet-RGB-Seg to IrrNet-Bi-Seg. The degree of improvement is also positively associated with the amount of levels (Supplementary File 5), which suggested that images with larger area coverage of contour-levee fields will likely to have increased accuracy with the inclusion of gradient steam. Finally, compared to RF and FCN-ATR-SKIP, respectively, our method improved 15% and 17% in *accuracy* and reduced 53% and 48% in *BER*. The consistently high accuracy of our model is suggested with the considerably low rate of *BER* at 0.33. Moreover, the improvement in *precision* (of 18% and 5.3%) and in *recall* (1.1% and 19.8%) also confirm the superior performance in this application.

Visualization of selected results shows how our model achieves the best match to the reference (Fig. 5). In contrast to RF and FCN-ATR-SKIP, our model demonstrates a meticulous segmentation of contour-levee fields with a homogeneous prediction for the crop fields. IrrNet-Bi produced less pixelated prediction and more agglomerated patches that depict the crop fields more realistically. The remaining isolated small patches that are most likely due to misclassification were further

removed by the superpixel post-processing.

4.3. Application: state-wide contour-levee field mapping

We predicted the contour-levee fields for the 27 agricultural counties in Arkansas (Fig. 6a). To better understand how the contour-levee system is used for rice cultivation and how it stands out among other irrigation methods, we calculated the latitudinal distribution of contour-levee fields, rice fields derived from the 2015 CDL, and irrigated land area derived from the 2015 LANID product. We summarized total acreage of contour-levee fields, rice fields, irrigated lands, and irrigated rice fields by county (Fig. 6c). The data of irrigated lands and irrigation by crop types were acquired from the Crop Acreage Data in the year 2015 (USDA Farm Service Agency, n.d.).

Across the latitudinal gradient, the distribution of contour-levee fields shares a similar pattern as the rice field coverage distribution (Fig. 6b). At the higher latitude (north of 35.5°N), the coverage of contour-levee fields is slightly lower than that of rice fields. Whereas in the lower latitude regions (south of 34.5°N), the two curves almost coincide. The high overlap between rice and contour-levee fields implies that, despite the higher water consumption, contour-levee irrigation is still the most dominant method in rice cultivation in the State of Arkansas. Besides rice, other crops such as soybean may also use contour-levee irrigation, which may result in their small acreage differences. The latitudinal distribution of our predicted contour-levee fields also follows the trend of the total irrigated land acreage. At the county scale, Poinsett, Cross, Arkansas County are the top three with the highest coverage of contour-levee fields (Fig. 6c). A more in-depth spatio-temporal analysis will be conducted in future studies.
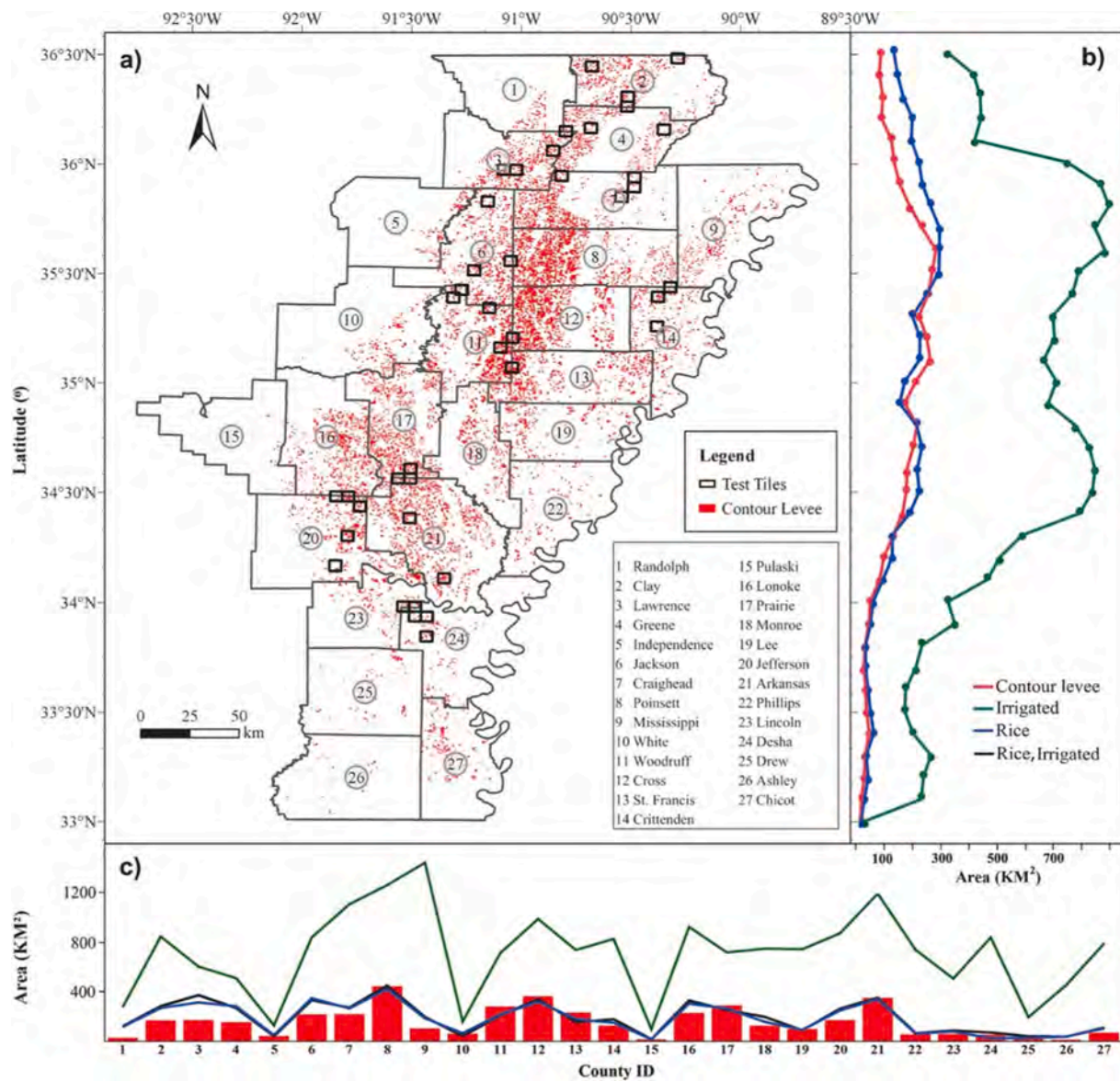
Fig. 6. a) The IrrNet-Bi-Seg predicted contour-levee field map for the Mississippi Alluvial Plain of Arkansas ; b) The latitudinal gradients in the area of contour-levee fields, rice fields, and irrigated lands in the mapped area of a). The x-axis is in km^2 per 0.1 decimal degree band; c) The total area of contour-levee fields, rice fields, irrigated lands, and irrigated rice fields, by county.
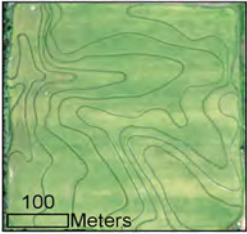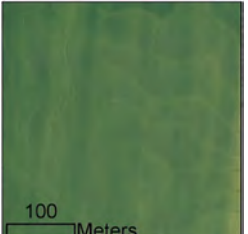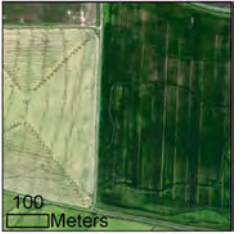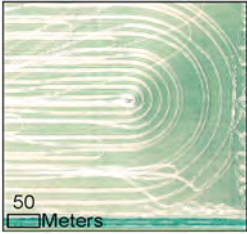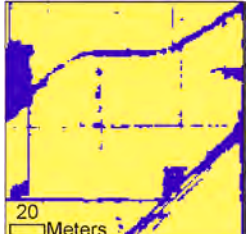
5. Discussion and perspectives

This research is the first field-scale, contour-levee irrigation type mapping activity by using a DL algorithm on high-resolution aerial imagery, and achieved satisfactory results based on the following observations: 1) The 16-fold validation showed overall accuracy of 0.90; 2) The independent test achieved an average accuracy of 0.86, demonstrating model generalizability and transferability; 3) IrrNet-Bi-Seg achieved 15% and 17% accuracy improvement over the benchmark methods; 4) Our latitudinal and county analysis is consistent with the reported USDA data.

Several improvements enhanced the model performance. The bi-stream network design fuses spectral information and the boundary pattern captured by gradients. Skip connection and deep supervision addresses the gradient vanishing problem. A previous study suggested that the deep supervision enhanced CNN model not only prevented overfitting but extracted features more transparently and outperformed several state-of-the-art methods by 2–7% (Muhammad et al., 2018).

Finally, superpixel-based majority voting suppressed noise generated in the IrrNet-Bi prediction. This step is critical to many agricultural applications that require accurate boundary depictions for making parcel-based crop or water management decisions (Cheng et al., 2020).

This work has made advances in both agricultural and remote sensing fields. One immediate application is that the work can justify focusing conservation programs in regions with the greatest proportional presence of contour-levee fields, such as Craighead, Poinsett, and Cross Counties (numbered 8, 12, 13 in Fig. 6). Such public- or private-sector programs could incentivize or otherwise encourage adaptation of water-saving irrigation pactices such as land-leveling, multiple inlet polypipe, or furrow irrigation (Massey et al., 2018; Reba and Massey, 2020). This work also suggests the future advancement of DL and remote sensing integration from a few perspectives: 1) it highlights the pressing need for standard training datasets that are customized for specific application needs; 2) remote sensing applications should align more closely with decision making activities. This work, in particular, will enable local (e.g., municipal) and regional (e.g., state and watershed)

Table 2
Illustration of four major challenges in irrigation practice mapping.

Dense	Sparse	Low	High
a. Levee spacing		b. Levee visibility	

c. Co-existing field patterns		d. Boundary detection	
Multi-class	Tractor path	Clear	Vague

water and agricultural management organizations, which may not otherwise have sufficient and consistent data resources to estimate irrigation system type, to make better decisions that influence regional water ability. 3) It presents many challenging tasks from some important aspects of remote sensing, as follows.

1) **Varying levee spacing**. Depending on field slope, levee spacing can vary from a very compact to a highly sparse form (Table 2a). In rare cases, the widest levee spacing exceeds the sliding window size of this study (300 × 300 pixels), leaving no line pattern in those captured views. We plan to adopt a multi-scale architecture, with inputs centered on the original input image but containing more geographic context. By aggregating features from various scales, the model may create a more informative set of features for model training.

2) **Vague representation of contour lines**. Levee visibility is a decisive factor in recognizing the irrigation system. Because the NAIP program acquires leaf-on imagery, the visibility of contour lines is impacted by high crop biomass (Table 2b). Problems arise when the trace of the levees is imperceptible and can barely be detected due to its similarity in color to the field. Image enhancement or different image sources from other time points may be adopted in future to strengthen the levee pattern. Higher weights may be given to the single gradient stream to weaken the influence of spectral information.

3) **Multiple patterns in one field** caused degraded annotation accuracy and model performance. One typical example is the co-presence of tractor trails with the levees when harvesting occurs earlier than the image acquisition dates (Table 2c). Additionally, some previously contour-levee fields were converted to furrow irrigation, yet levee traces are still distinct (Table 2c right). Intensive field land modification associated with the high rotation rate of rice also adds complexity to the pattern interpretation. About 72% of the state's rice acreage will be rotated into soybeans and will likely to be modified to furrow, center-pivot, or straight-levee (Kebede et al., 2014). In a follow-up study, we plan to incorporate existing information on crop cover type and irrigation status maps to support annotation and modeling.

4) **Better boundary detection methods for improved superpixel quality**. We demonstrated the superiority of integrating superpixels for improved model performance. However, in some cases where the segmented superpixels are inaccurate, the errors are propagated into prediction (Table 2d). These undesirable shapes may not significantly decrease accuracy but limit the use of such mapping products in applications that require precise crop field boundaries. We plan to apply advanced techniques, such as Conditional Random Field, which considers the spatial relations between the labeled pixels modeled in form of a graph.

6. Conclusion

A comprehensive understanding of agriculture-induced water consumption is critical to meet the growing need for agricultural products amid increasing competition with industry and municipalities. In this work, we proposed IrrNet-Bi-Seg that integrates augmented training samples, skip connection, deep supervision, and superpixel postprocessing, which, together, provides new perspectives on using DL approaches for crop irrigation type mapping. With this method structure, field-scale mapping of the contour-levee fields in the MAP region of Araksans was accomplished. Given the size and coverage, this work could be adapted for larger-scale studies and be tested for multiple irrigation type mapping.

CRediT authorship contribution statement

Lu Liang: Conceptualization, Methodology, Visualization, Writing – original draft, Project administration. **Abolfazl Meyarian:** Methodology, Formal analysis, Writing – original draft. **Xiaohui Yuan:** Methodology, Formal analysis, Writing – review & editing. **Benjamin R.K. Runkle:** Investigation, Resources, Writing – review & editing. **George Mihaila:** Software, Writing – review & editing. **Yuchu Qin:** Software. **Jacob Daniels:** Visualization. **Michele L. Reba:** Investigation, Resources. **James R. Rigby:** Resources, Funding acquisition.

Declaration of Competing Interest

The authors declare that they have no known competing financial interests or personal relationships that could have appeared to influence the work reported in this paper.

Appendix A. Supplementary data

Supplementary data to this article can be found online at https://doi.org/10.1016/j.jag.2021.102631.

References

Achanta, R., Shaji, A., Smith, K., Lucchi, A., Fua, P., Süsstrunk, S., 2010. SLIC superpixels. Tech. Rep, EPFL.

Artstein, R., Poesio, M., 2008. Inter-Coder Agreement for Computational Linguistics. Comput. Linguist. 34 (4), 555–596. https://doi.org/10.1162/coli.07-034-R2.

Breiman, L., 2001. Random Forests. Mach. Learn. 45, 5–32. https://doi.org/10.1023/A:1010933404324.

California Rice Production Workshop, 2018. Land Formation.

Cheng, T., Ji, X., Yang, G., Zheng, H., Ma, J., Yao, X., Zhu, Y., Cao, W., 2020. DESTIN: A new method for delineating the boundaries of crop fields by fusing spatial and temporal information from WorldView and Planet satellite imagery. Comput. Electron. Agric. 178, 105787. https://doi.org/10.1016/j.compag.2020.105787.

Cohen, J., 1960. A Coefficient of Agreement for Nominal Scales. Educ. Psychol. Meas. 20 (1), 37–46. https://doi.org/10.1177/001316446002000104.

Dieter, C.A., Maupin, M.A., Caldwell, R.R., Harris, M.A., Ivahnenko, T.I., Lovelace, J.K., Barber, N.L., Linsey, K.S., 2018. Estimated use of water in the United States in 2015 (USGS Numbered Series No. In: 1441), Estimated use of water in the United States in 2015, Circular. U.S. Geological Survey. https://doi.org/10.3133/cir1441.

Felzenszwalb, P.F., Huttenlocher, D.P., 2004. Efficient Graph-Based Image Segmentation. Int. J. Comput. Vis. 59 (2), 167–181. https://doi.org/10.1023/B:VISI.0000022288.19776.77.

Gosling, Simon N., Arnell, Nigel W., 2016. A global assessment of the impact of climate change on water scarcity. Clim. Change 134 (3), 371–385. https://doi.org/10.1007/s10584-013-0853-x.

Henry, C.G., Hirsh, S.L., Anders, M.M., Vories, E.D., Reba, M.L., Watkins, K.B., Hardke, J.T., 2016. Annual Irrigation Water Use for Arkansas Rice Production. J. Irrig. Drain. Eng. 142 (11), 05016006. https://doi.org/10.1061/(ASCE)IR.1943-4774.0001068.

Hsiao, Theodore C., Steduto, Pasquale, Fereres, Elias, 2007. A systematic and quantitative approach to improve water use efficiency in agriculture. Irrig. Sci. 25 (3), 209–231. https://doi.org/10.1007/s00271-007-0063-2.

Huang, G., Liu, Z., van der Maaten, L., Weinberger, K.Q., 2018. Densely Connected Convolutional Networks. ArXiv160806993 Cs.

Jawak, Shridhar D., Devliyal, Prapti, Luis, Alvarinho J., 2015. A Comprehensive Review on Pixel Oriented and Object Oriented Methods for Information Extraction from Remotely Sensed Satellite Images with a Special Emphasis on Cryospheric Applications. Adv. Remote Sens. 04 (03), 177–195. https://doi.org/10.4236/ars.2015.43015.

Kebede, Hirut, Fisher, Daniel K., Sui, Ruixiu, Reddy, Krishna N., 2014. Irrigation Methods and Scheduling in the Delta Region of Mississippi: Current Status and Strategies to Improve Irrigation Efficiency. Am. J. Plant Sci. 05 (20), 2917–2928. https://doi.org/10.4236/ajps.2014.520307.

Ketchum, D., Jencso, K., Maneta, M.P., Melton, F., Jones, M.O., Huntington, J., 2020. IrrMapper: A Machine Learning Approach for High Resolution Mapping of Irrigated Agriculture Across the Western U.S. Remote Sens. 12, 2328. https://doi.org/10.3390/rs12142328.

Liang, L., Hawbaker, T.J., Zhu, Z., Li, X., Gong, P., 2016. Forest disturbance interactions and successional pathways in the Southern Rocky Mountains. For. Ecol. Manag. 375, 35–45. https://doi.org/10.1016/j.foreco.2016.05.010.

Liang, Lu, Runkle, Benjamin R.K., Sapkota, Bishwa B., Reba, Michele L., 2019. Automated mapping of rice fields using multi-year training sample normalization. Int. J. Remote Sens. 40 (18), 7252–7271. https://doi.org/10.1080/01431161.2019.1601286.

Massey, Joseph H., Mark Stiles, C., Epting, Josh W., Shane Powers, R., Kelly, David B., Bowling, Taylor H., Leighton Janes, C., Pennington, Dean A., 2017. Long-term measurements of agronomic crop irrigation made in the Mississippi delta portion of the lower Mississippi River Valley. Irrig. Sci. 35 (4), 297–313. https://doi.org/10.1007/s00271-017-0543-y.

Massey, J.H., Smith, M.C., Vieira, D.A.N., Adviento-Borbe, M.A., Reba, M.L., Vories, E.D., 2018. Expected Irrigation Reductions Using Multiple-Inlet Rice Irrigation under Rainfall Conditions of the Lower Mississippi River Valley. J. Irrig. Drain. Eng. 144 (7), 04018016. https://doi.org/10.1061/(ASCE)IR.1943-4774.0001303.

Mboga, N., Grippa, T., Georganos, S., Vanhuysse, S., Smets, B., Dewitte, O., Wolff, E., Lennert, M., 2020. Fully convolutional networks for land cover classification from historical panchromatic aerial photographs. ISPRS J. Photogramm. Remote Sens. 167, 385–395. https://doi.org/10.1016/j.isprsjprs.2020.07.005.

Meyarian, Abolfazl, Yuan, Xiaohui, Liang, Lu, Wang, WenCheng, Gu, Lichuan, 2021. Gradient convolutional neural network for classification of agricultural fields with contour levee. Int. J. Remote Sens. (in press).

Mi, L., Chen, Z., 2020. Superpixel-enhanced deep neural forest for remote sensing image semantic segmentation. ISPRS J. Photogramm. Remote Sens. 159, 140–152. https://doi.org/10.1016/j.isprsjprs.2019.11.006.

Molden, D., International Water Management Institute, Comprehensive Assessment of Water Management in Agriculture (Program) (Eds.), 2007. Water for food, water for life: a comprehensive assessment of water management in agriculture. Sterling, VA, Earthscan, London.

Moreno-García, Beatriz, Coronel, Eric, Reavis, Colby W., Suvočarev, Kosana, Runkle, Benjamin R.K., 2021. Environmental sustainability assessment of rice management practices using decision support tools. J. Clean. Prod. 315, 128135. https://doi.org/10.1016/j.jclepro.2021.128135.

Muhammad, U., Wang, W., Hadid, A., 2018. Feature Fusion with Deep Supervision for Remote-Sensing Image Scene Classification. In: in: 2018 IEEE 30th International Conference on Tools with Artificial Intelligence (ICTAI). Presented at the 2018 IEEE 30th International Conference on Tools with Artificial Intelligence (ICTAI), pp. 249–253. https://doi.org/10.1109/ICTAI.2018.00046.

Neubert, P., Protzel, P., 2014. Compact Watershed and Preemptive SLIC: On Improving Trade-offs of Superpixel Segmentation Algorithms. In: International Conference on Pattern Recognition. Presented at the 2014 22nd International Conference on Pattern Recognition, pp. 996–1001. https://doi.org/10.1109/ICPR.2014.181.

Pervez, M.S., Brown, J.F., 2010. Mapping Irrigated Lands at 250-m Scale by Merging MODIS Data and National Agricultural Statistics. Remote Sens. 2, 2388–2412. https://doi.org/10.3390/rs2102388.

Reba, M.L., Massey, J.H., 2020. Surface Irrigation in the Lower Mississippi River Basin: Trends and Innovations. Trans. ASABE 63, 1305–1314. https://doi.org/10.13031/trans.13970.

Ronneberger, O., Fischer, P., Brox, T., 2015. U-Net: Convolutional Networks for Biomedical Image Segmentation. ArXiv150504597 Cs.

Rundquist, D., Hoffman, R.O., Carlson, M., Cook, A.E., 1989. The Nebraska center-Pivot inventory : an example of operational satellite remote sensing on a long-term basis. Photogramm. Eng. Remote Sens. 55, 587–590.

Salamati, N., Larlus, D., Csurka, G., Süsstrunk, S., 2012. Semantic Image Segmentation Using Visible and Near-Infrared Channels, in: Fusiello, A., Murino, V., Cucchiara, R. (Eds.), Computer Vision – ECCV 2012. Workshops and Demonstrations, Lecture Notes in Computer Science. Springer, Berlin, Heidelberg, pp. 461–471. https://doi.org/10.1007/978-3-642-33868-7_46.

Stojmenović, Miloš, Žunić, Joviša, 2008. Measuring Elongation from Shape Boundary. J. Math. Imaging Vis. 30 (1), 73–85. https://doi.org/10.1007/s10851-007-0039-0.

Thenkabail, Prasad S., Biradar, Chandrashekhar M., Noojipady, Praveen, Dheeravath, Venkateswarlu, Li, Yuanjie, Velpuri, Manohar, Gumma, Muralikrishna, Gangalakunta, Obi Reddy P., Turral, Hugh, Cai, Xueliang, Vithanage, Jagath, Schull, Mitchell A., Dutta, Rishiraj, 2009. Global irrigated area map (GIAM), derived from remote sensing, for the end of the last millennium. Int. J. Remote Sens. 30 (14), 3679–3733. https://doi.org/10.1080/01431160802698919.

Tkachenko, M., Malyuk, M., Shevchenko, N., Holmanyuk, A., Liubimov, N., 2020. Label Studio: Data labeling software.

United Nations Educational, Scientific and Cultural Organization, 2014. Fact 24: Irrigated land [WWW Document]. URL http://www.unesco.org/new/en/natural-sciences/environment/water/wwap/facts-and-figures/all-facts-wwdr3/fact-24-irrigated-land/ (accessed 7.15.21).

USDA Farm Service Agency, n.d. Crop Acreage Data - 2015 Crop Year [WWW Document]. Natl.-Content. URL https://fsa.usda.gov/news-room/efoia/electronic-reading-room/frequently-requested-information/crop-acreage-data/index (accessed 8.3.21).

USDA/NASS 2020 State Agriculture Overview for Arkansas [WWW Document], 2020. URL https://www.nass.usda.gov/Quick_Stats/Ag_Overview/stateOverview.php?state=ARKANSAS (accessed 7.15.21).

Vedaldi, A., Soatto, S., 2008. Quick Shift and Kernel Methods for Mode Seeking. In: Forsyth, D., Torr, P., Zisserman, A. (Eds.), Computer Vision – ECCV 2008. Springer, Berlin Heidelberg, Berlin, Heidelberg, pp. 705–718.

Vories, E.D., Tacker, P.L., Hogan, R., 2005. Multiple inlet approach to reduce water requirements for rice production. Appl. Eng. Agric. 21, 611–616. https://doi.org/10.13031/2013.18571.

Wilson, C.E., Branson, J.W., 2004. Trends in Arkansas Rice Production 60.

Xie, S., Tu, Z., 2015. Holistically-Nested Edge Detection. ArXiv150406375 Cs.

Xie, Y., Gibbs, H.K., Lark, T.J., 2021. Landsat-based Irrigation Dataset (LANID): 30-m resolution maps of irrigation distribution, frequency, and change for the U.S., 1997–2017 (preprint). Data, Algorithms, and Models. https://doi.org/10.5194/essd-2021-207.

Yan, L., Roy, D.P., 2014. Automated crop field extraction from multi-temporal Web Enabled Landsat Data. Remote Sens. Environ. 144, 42–64. https://doi.org/10.1016/j.rse.2014.01.006.

Yang, J., Ren, W., Ouyang, Y., Feng, G., Tao, B., Granger, J.J., Poudel, K.P., 2019a. Projection of 21st century irrigation water requirement across the Lower Mississippi Alluvial Valley. Agric. Water Manag. 217, 60–72. https://doi.org/10.1016/j.agwat.2019.02.033.

Yang, Lingbo, Mansaray, Lamin, Huang, Jingfeng, Wang, Limin, 2019b. Optimal segmentation scale parameter, feature subset and classification algorithm for geographic object-based crop recognition using multisource satellite imagery. Remote Sens. 11 (5), 514. https://doi.org/10.3390/rs11050514.